Unidirectional multipulse helicity-independent all-optical switching in [Ni/Pt] based synthetic ferrimagnets

Connor R. J. Sait,[1] Maciej Dąbrowski,[1] Jade N. Scott,[2] William R. Hendren,[2] David G. Newman,[1] Alpha T. N'Diaye,[3] Christoph Klewe,[3] Padraic Shafer,[3] Gerrit van der Laan,[4] Paul S. Keatley,[1] Robert M. Bowman,[2] and Robert J. Hicken[1]

[1]*Department of Physics and Astronomy, University of Exeter, Stocker Road, EX4 4QL, United Kingdom*
[2]*School of Mathematics and Physics, Queen's University Belfast, Belfast, BT7 1NN, United Kingdom*
[3]*Advanced Light Source, Lawrence Berkeley National Laboratory, Berkeley, California, 94720, USA*
[4]*Diamond Light Source, Harwell Science and Innovation Campus, Didcot, OX11 0DE, United Kingdom*

(Received 3 August 2023; accepted 11 March 2024; published 11 April 2024)

Nickel-platinum-based synthetic ferrimagnets (SFi's) are highly tunable and rare-earth-free materials that allow ultrafast all optical control of magnetism to be explored. This study considers a SFi composed of a ferromagnetic [Ni/Pt] multilayer and a ferromagnetic Co layer, separated by an Ir layer that mediates an antiferromagnetic coupling. Helicity-independent all optical switching (HI-AOS) between two antiparallel magnetization states is observed. AOS may be realized at increased temperature through reduction of the thickness of the Pt layers. Switching is unidirectional and has a strong dependence on the applied magnetic field history, which suggests the possible presence of a nanoscale magnetic texture that may be important in controlling AOS in SFi systems.

DOI: 10.1103/PhysRevB.109.134417

I. INTRODUCTION

Ultrafast all optical switching (AOS) of magnetic materials has attracted great interest as a potential solution to the magnetic recording trilemma [1,2]. The observation of subpicosecond demagnetization in nickel [3] initiated a search for more general optical control of magnetization in the absence of an applied magnetic field. In general, AOS can be divided into two categories: helicity-independent AOS (HI-AOS) and helicity-dependent AOS (HD-AOS). HD-AOS has been principally driven by magnetic circular dichroism (MCD) [4,5], and can be observed in various materials including ferromagnetic layers [6–11] and rare-earth (RE)-free synthetic ferrimagnets (SFi's) [12,13], but requires multiple pulses. In contrast, HI-AOS can be achieved with a single pulse, and occurs as a result of an exchange of angular momentum between two ferrimagnetic sublattices [14–16]. For a long time HI-AOS was only observed in ferrimagnetic rare-earth transition-metal (RE-TM) alloys [4,17–21], and SFi's [22–24] and spin valves [25] containing RE atoms. More recently, HI-AOS has been demonstrated in other materials such as a ferrimagnetic Heusler alloy [26], cobalt-substituted yttrium iron garnet [27], a ferromagnetic spin valve [28], and a two-dimensional (2D) van der Waals magnet [29].

From the viewpoint of technological applications, RE-free SFi's are highly attractive due to the low cost and relative abundance of the constituent materials, and their unparalleled tunability [30]. However, RE-free SFi's containing chemically dissimilar layers remain largely unexplored, with HI-AOS so far only being achieved in Ni_3Pt/Ir/Co [31], where the Ni_3Pt layer was grown at elevated temperature to induce perpendicular magnetic anisotropy (PMA). Time-resolved measurements of the ultrafast demagnetization process suggested that the HI-AOS is driven by spin-polarized current passing through the Ir spacer layer. However, multiple pulses with a high repetition rate were needed for switching to occur.

Theory suggests that the interlayer exchange coupling (IEC) between the ferromagnetic layers should exceed 6 mJ/m^2 to achieve single-pulse switching within a SFi [30]. Here we examine the properties of [Ni/Pt]/Ir/Co SFi's, where use of a [Ni/Pt] multilayer results in larger switching fields that imply larger IEC, and increased values of the so-called negative remanence temperature T_{-R} and magnetic compensation temperature T_M. A correlation between the negative remanence temperature and optically induced magnetization switching was established in Ref. [31], where it was shown that HI-AOS only occurs below T_{-R}. While the reasons for this correlation are still being explored, it suggests that increased T_{-R} will be needed to achieve HI-AOS at higher temperatures for nickel-platinum-based SFi's. The measurements reported here suggest that the HI-AOS is a two-step process that involves both an internal flow of spin current and a more gradual growth of switched domains. Furthermore, this switching is found to be both unidirectional and sensitive to the detailed field history through which the initial remanent state is prepared.

II. EXPERIMENTAL METHOD

The magnetic state of each sample was imaged via the polar magnetooptical Kerr effect (MOKE) in a wide-field

Kerr microscope (WFKM) equipped with a linearly polarized white light LED source. A pulsed ultrafast laser of 1035 nm wavelength, with pulse width variable between 280 fs and 10 ps, and repetition rate variable between 10 kHz and 1 MHz, was introduced to the microscope setup and the beam was brought to the sample surface at 45 degree angle of incidence. The beam was passed through a linear polarizer, a half-wave-plate and a quarter-wave-plate to set the fluence and polarization of the laser pulses prior to arrival at the sample. A mirror and a lens were used to focus the beam onto the area of the sample surface within the focal plane of the microscope. A predetermined number of pulses was applied to the sample by using a function generator with variable trigger times to provide a gating signal.

A superconducting quantum interference device (SQUID) magnetometer was used to determine the magnetization of the SFi samples. Hysteresis loops were acquired with an out-of-plane applied field. Two different procedures were used to determine the remanent magnetization as a function of temperature. In the first case, the magnetization was prepared at each temperature point by applying a saturating field and then reducing the field again to zero. In the second case, the remanent state was prepared in the same manner at 10 K, and then the magnetization was measured as the temperature was increased. As shown in Figs. S1–S3 in the Supplemental Material [32], the rate at which the applied field is swept from saturation to remanence can effect the resulting remanent state through changes to the magnetization reversal dynamics, in agreement with Ref. [33].

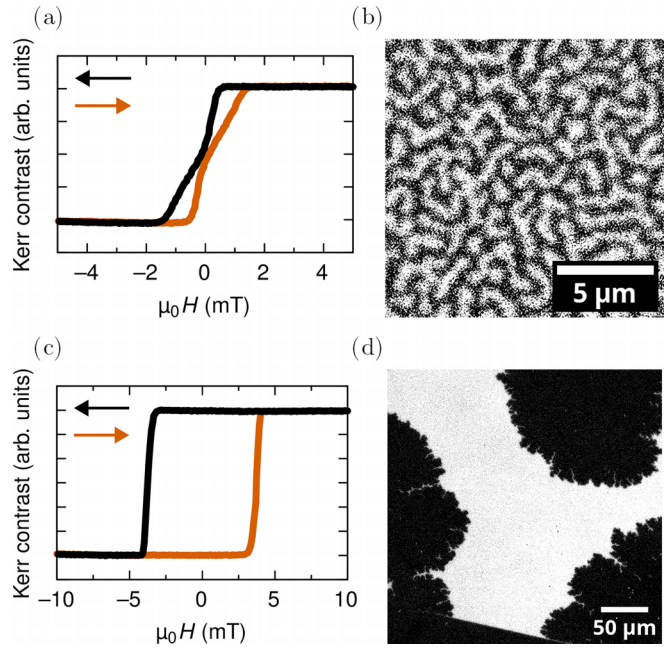

FIG. 1. Comparison of the field-induced switching of [Ni/Pt] reference layers at room temperature. (a) shows the WFKM measured hysteresis loop of the $[Ni/Pt]_A$ reference stack, which relaxes into a multidomain state at remanence as shown in (b). (c) shows the loop for $[Ni/Pt]_B$ with the domains observed at the coercive field of −4 mT shown in (d).

III. MULTILAYER REFERENCE SAMPLES

To understand the magnetic properties of the [Ni/Pt] multilayer, Pt(5 nm)/6×[Ni(0.6 nm/Pt(X)]/Pt(5 nm) structures with $X = 0.3$ and 0.25 nm, referred to as $[Ni/Pt]_A$ and $[Ni/Pt]_B$, respectively, were deposited by RF and DC sputtering at RT from elemental targets onto c-plane Al_2O_3 substrates. Sputtering was performed in an Ar^+ environment with a base pressure of 10^{-9} torr and sputtering pressure of 10^{-3} torr.

Figure 1 shows WFKM hysteresis loops [Figs. 1(a), 1(c)] and domain images [Figs. 1(b), 1(d)] at 297 K, with significantly different behavior observed due to the small change in Pt thickness. First, the domains are two orders of magnitude smaller in $[Ni/Pt]_A$, appearing on the scale of approximately 1 µm, as opposed to 100 µm in $[Ni/Pt]_B$. Second, the saturation field of $[Ni/Pt]_A$ (∼2 mT) is less than half that of $[Ni/Pt]_B$ (∼5 mT). The $[Ni/Pt]_A$ loop has a wasp-waist shape due to domains forming at remanence to reduce the dipolar energy. This behavior is not seen in $[Ni/Pt]_B$, where the loop takes a square shape with a coercive field of about 4 mT.

Images of the domains in $[Ni/Pt]_B$ at various temperatures (Fig. S4 [32]) show a decrease in the size of the domains as the temperature is increased towards 330 K. The structure of both the domains and hysteresis loops (Fig. S5 [32]) collapse at 330 K becoming more similar to the results for $[Ni/Pt]_A$ at room temperature. The temperature-dependent properties of $[Ni/Pt]_A$ and $[Ni/Pt]_B$ are similar but with $[Ni/Pt]_B$ exhibiting a larger Curie temperature, presumably because the exchange interaction between the Ni layers is increased by reducing the Pt thickness.

IV. SFI SAMPLES

Pt(5 nm)/[Ni(0.6 nm)/Pt(X)]$_5$/Ni(0.6 nm)/Ir(0.4 nm)/Co (0.8 nm)/Ir(3 nm) structures, with $X = 0.3$ and 0.25 nm for SFi samples A and B, respectively, were grown at RT. The [Ni/Pt] and Co layers are separated by an Ir spacer layer, through which an antiferromagnetic IEC occurs due to the RKKY interaction [34–37].

A field of sufficient magnitude will saturate SFi samples by causing the parallel (P) alignment of the ferromagnetic layers into a state labeled $\mathbf{P}^+$. At remanence, the moments of the [Ni/Pt] and Co layers align antiparallel (AP) in one of two arrangements labeled $\mathbf{AP}^+$ and $\mathbf{AP}^-$. Below T_M, the point at which the magnetic moments of the two FM layers cancel, $\mathbf{AP}^+$ ($\mathbf{AP}^-$) denotes the case where the larger moment remains parallel (antiparallel) to the previously applied field. In what follows the labels refer to the case that the field is swept from positive to negative.

Hysteresis loops obtained from SQUID magnetometry measurements for the two samples are shown in Fig. 2. Loops for sample A are shown at temperatures of [Fig. 2(a)] 250 K and [Fig. 2(b)] 300 K. In Fig. 2(b) the magnetization takes a negative value indicating an $\mathbf{AP}^-$ state when the field is swept from positive saturation to remanence, exhibiting the so-called negative remanence behavior. Loops for sample B are shown at [Fig. 2(c)] 325 K and [Fig. 2(d)] 330 K.

Element specific hysteresis loops, obtained from x-ray magnetic circular dichroism (XMCD) measurements, for the

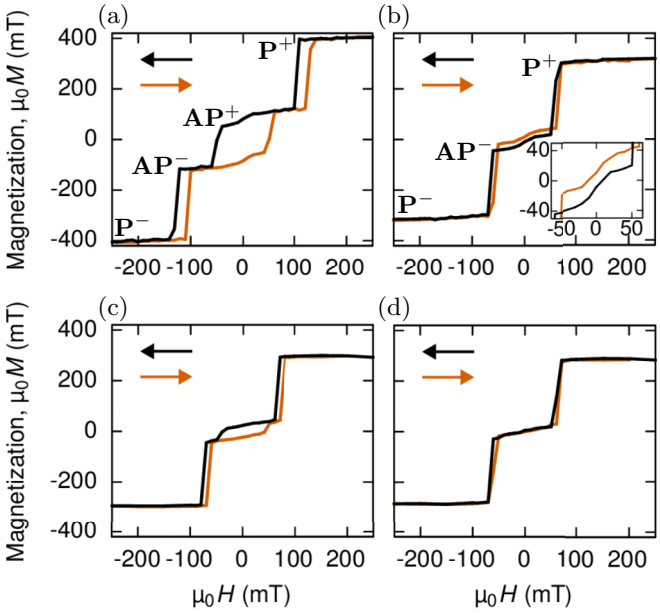

FIG. 2. Hysteresis loops obtained from SQUID magnetometry measurements show (a) positive remanence at 250 K, and (b) negative remanence at 300 K for sample A, and (c) positive remanence at 325 K and (d) negative remanence at 330 K for sample B. The parallel **P** and antiparallel **AP** states obtained when sweeping the field from positive to negative saturation (the black section of the loops) have been labeled in (a) and (b).

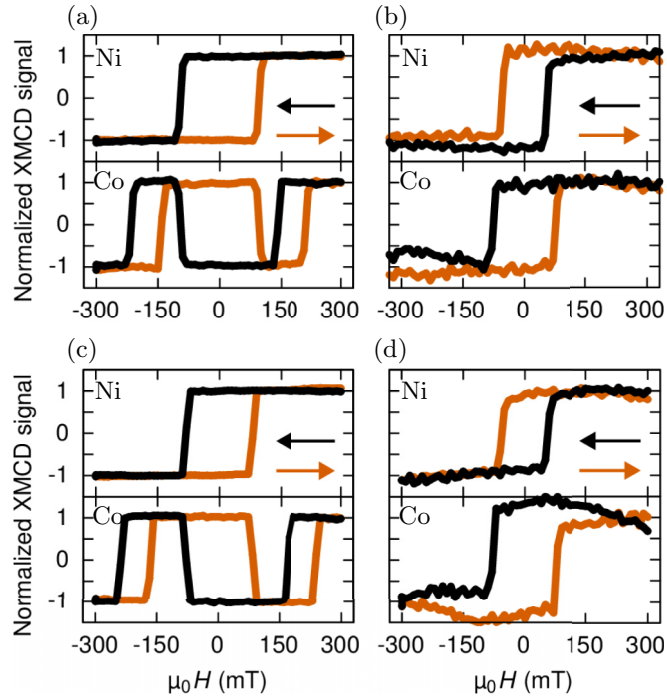

FIG. 3. Element specific XMCD hysteresis loops measured at the Ni L_3 (851.79 eV) and Co L_3 (777.94 eV) x-ray absorption edges. For sample A the loops show (a) positive remanence at 200 K and (b) negative remanence at 300 K. For sample B, they show (c) positive remanence at 200 K and (d) negative remanence at 330 K. The black lines show the effect of sweeping the magnetic field in the negative direction, while the orange lines show the effect of sweeping in the positive direction.

coupled Co and [Ni/Pt] layers are shown in Fig. 3. Loops for sample A are shown at temperatures of [Fig. 3(a)] 200 K and [Fig. 3(b)] 300 K for which positive and negative remanence, respectively, are observed in SQUID measurements. Comparable loops for sample B are shown at [Fig. 3(c)] 200 K and [Fig. 3(d)] 330 K. At temperatures where negative remanence behavior is observed, the Co undergoes a single switching event and the [Ni/Pt] switches before rather than after reaching remanence when coming from a saturated state. The single reversal of Co at higher temperatures is due to its magnetic anisotropy being relatively larger compared to that of the [Ni/Pt] [38], and results in a negative remanence state. Below T_{-R} the Co layer exhibits multiple switching events due to competition between the Zeeman, IEC, and magnetic anisotropy energies. From these measurements it can be seen that [Ni/Pt] has the larger moment below T_M, as it remains aligned in the direction of the previously applied field below T_{-R}.

The coercivities of the SFi samples are an order of magnitude larger than those of the reference layers due to the antiferromagnetic coupling of the layers within the SFi. The relative size of the layer moments is strongly temperature dependent, with full compensation at T_M. This leads to a variation in the coercivity of the SFi samples, with a moderate increase being observed as the temperature approaches T_M from below [39].

Both SFi's display negative remanence for a range of temperatures bounded by the negative remanence temperature T_{-R} and compensation temperature T_M. This range is shown in Fig. 4 for [Fig. 4(a)] sample A and [Fig. 4(b)] sample B, where, the remanent magnetization determined from the SQUID measurements described in Sec. II are plotted against temperature. The negative remanence regime corresponds to the range of temperatures shaded orange. Within this regime, negative remanence occurs because it is more energetically favorable to switch the ferromagnetic layer with the larger moment to achieve antiparallel alignment as the applied field is decreased towards remanence [40].

The multilayer structure of the [Ni/Pt] allows the magnetic properties of the SFi to be tuned. It was found that the thickness of the Pt layers determines the values of T_{-R} and T_M, with T_{-R} increasing from $T_{-R}^A = 289$ K to $T_{-R}^B = 326$ K, and T_M increasing from $T_M^A = 310$ K to $T_M^B = 343$ K, as the Pt layer thickness was reduced by 0.05 nm.

Returning to Figs. 2 and 3, the remanence behavior in each loop matches that shown in Fig. 4, except for that shown in Fig. 2(d). Here, within the negative remanence regime for sample B, the remanent magnetization is shown to collapse rather than take a negative value. This discrepancy results from the slower rate at which the field was swept in the SQUID hysteresis loop measurements, which in this case allows for formation of equal numbers of $\mathbf{AP}^+$ and $\mathbf{AP}^-$ domains as deduced from Figs. S1–S3 [32].

The size of the domains in the $[\mathrm{Ni/Pt}]_B$ reference multilayer collapses close to T_{-R}^B (see Fig. S4 [32]). This suggests that the temperature dependent properties of the [Ni/Pt] stack are the principal driver for the negative remanence behavior.

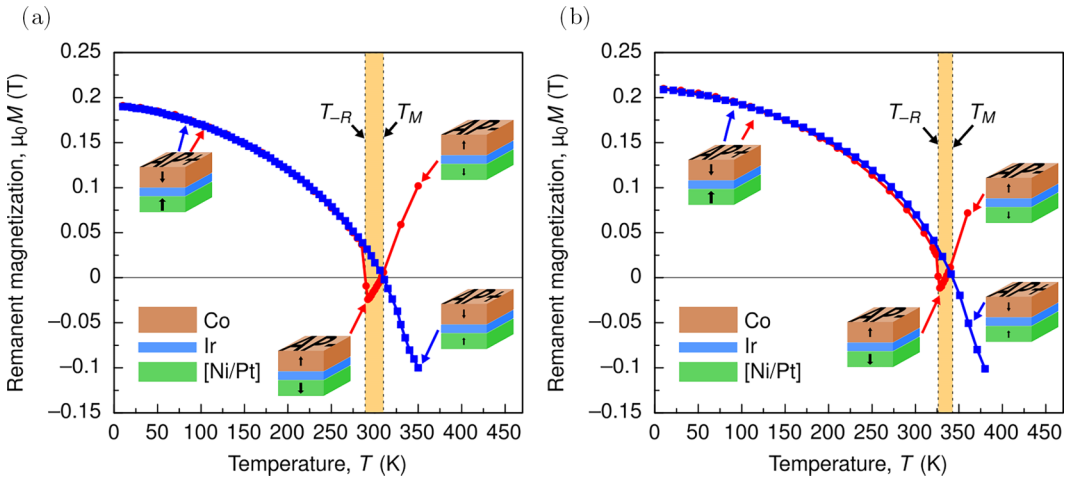

FIG. 4. Dependence of remanent magnetization on temperature as determined by SQUID magnetometry. Red circles show the remanent magnetization measured after saturation followed by immediate removal of the field at each temperature. Blue squares show how the remanent magnetization changes after preparing the remanent state at 10 K and then increasing the temperature. The type of antiferromagnetic alignment, $\mathbf{AP}^+$ or $\mathbf{AP}^-$, is indicated for each region. Results are shown for (a) sample A where the negative remanence regime falls between $T^A_{-R} = 289$ K and $T^A_M = 310$ K and for (b) sample B where the negative remanence regime falls between $T^B_{-R} = 326$ K and $T^B_M = 343$ K.

Negative remanence occurs when the ferromagnetic layer with the smaller moment has much larger anisotropy and hence coercivity than the ferromagnetic layer with the larger moment. This is confirmed by comparison of the collapsed coercivity in $[\mathrm{Ni/Pt}]_\mathrm{A}$ [Fig. 1(a)] with the 6 mT coercivity of the square Co loop at RT (shown in Fig. S6 [32]).

Compared to SFi's with a Ni_3Pt alloy layer [31], the antiferromagnetic type IEC mediated by the Ir is increased from 0.03 $\mathrm{mJ/m^2}$ to 0.08 $\mathrm{mJ/m^2}$. The enhancement is revealed by comparing the size of the switching fields [40], although differences in the PMA, which tends to be smaller for the multilayer, must be accounted for before the IEC can be properly quantified.

A number of factors influence the strength of the IEC, chiefly the properties of the interlayer separating the FM layers. Compared to the previous study on Ni_3Pt based SFi's [31], the thickness of the Ir layer which couples the FM layers was reduced from 0.5 to 0.4 nm which was found to give the maximum IEC. The switching and saturation fields at RT are approximately doubled, indicating a similar enhancement of the IEC. The main contribution to this enhancement is thought to arise from improved structural quality of the [Ni/Pt]/Ir interface owing to changes in the growth procedure. PMA is achieved in multilayer [Ni/Pt] in a single-stage sputtering process at RT, whereas Ni_3Pt must first be deposited at elevated temperatures to obtain PMA.

V. WIDE FIELD KERR MICROSCOPE LOOPS AND MICROMAGNETIC STATES

The difference in magnetic behavior above and below T_{-R} is explored further in Fig. 5, where the magnetic contrast obtained from WFKM images of a 0.2 $\mathrm{mm^2}$ area of the SFi are presented. By comparison with the XMCD loops in Fig. 3, the available equilibrium states can be inferred, along with the field history required to form them. Domains that form during switching events are shown beside the spatially averaged loops in Fig. 5 where states of parallel **P** and antiparallel **AP** aligned FM layers are labeled along the field path swept from positive to negative saturation. Slightly below T^A_{-R} at 285 K, in Fig. 5(a), when moving from positive saturation at +104 mT to negative saturation at −104 mT, the first switching event is $\mathbf{P}^+ \rightarrow \mathbf{AP}^+$ at +78 mT [domains in Fig. 5(e)]. The next event to occur is $\mathbf{AP}^+ \rightarrow \mathbf{AP}^-$ at −67 mT [Fig. 5(f)]. As a result of event $\mathbf{AP}^- \rightarrow \mathbf{P}^-$ [Fig. 5(g)] the magnetization is again saturated beyond −101 mT. Slightly above T_{-R} [Fig. 5(b)], within the negative remanence regime, $\mathbf{P}^+ \rightarrow \mathbf{AP}^-$occurs at 71 mT [Fig. 5(h)], leading to negative remanence at 0 mT. Event $\mathbf{AP}^- \rightarrow \mathbf{P}^-$ occurs at −90 mT [Fig. 5(i)] and involves domains of size similar to those seen for the similar transition below T_{-R} [Fig. 5(g)].

Events $\mathbf{P}^+ \rightarrow \mathbf{AP}^+$ and $\mathbf{AP}^+ \rightarrow \mathbf{AP}^-$ involve Co layer switching, and simultaneous reversal of both FM layers, respectively. These events produce large domains about 100 μm in size. Small domains of tens of μm in size nucleate when the Co layer switches for $\mathbf{AP}^- \rightarrow \mathbf{P}^-$ and even smaller domains of the order of 1 μm in size nucleate as the [Ni/Pt] layer switches for $\mathbf{P}^+ \rightarrow \mathbf{AP}^-$.

VI. ALL-OPTICAL SWITCHING

For the [Ni/Pt]-based SFi's studied here, ultrafast laser pulses focused to a Gaussian spot of 116 μm ($1/e^2$) diameter were found to modify the magnetic state above a critical threshold fluence. This threshold and the induced magnetic changes both depend on various factors including temperature, pulse width, and pulse repetition rate. For the majority of the parameter space, optical pumping with sufficient fluence results in thermal demagnetization of the exposed region and formation of domains. Below T_{-R}, higher temperature and higher pulse repetition rate generally lead to domains of increased size, while for optimized parameter values the domains join completely resulting in HI-AOS between AP states. For conditions that result in AOS, further increase of fluence destroys the effect and instead results in thermal demagnetization (Fig. S7 [32]). Eventually, continued increase

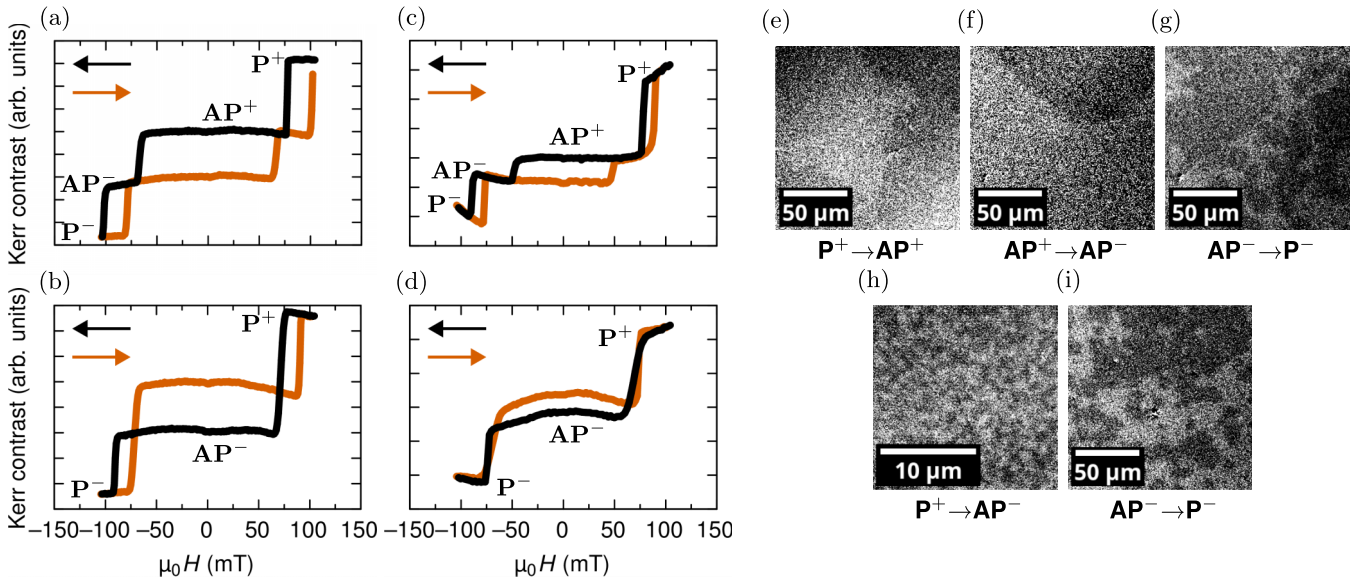

FIG. 5. Spatially averaged Kerr hysteresis loops showing (a) positive remanence at 285 K and (b) negative remanence at 293 K for sample A, and (c) positive remanence at 330 K and (d) negative remanence at 338 K for sample B. States are labeled for the decreasing field (black) sections of the loops. WFKM images of the switching events in sample A show the formation of large domains for (e) $\mathbf{P}^+ \rightarrow \mathbf{AP}^+$ and (f) $\mathbf{AP}^+ \rightarrow \mathbf{AP}^-$, both at 285 K, small domains for (g), (i) $\mathbf{AP}^- \rightarrow \mathbf{P}^-$, at 285 K and 293 K respectively, and minuscule domains for (h) $\mathbf{P}^+ \rightarrow \mathbf{AP}^-$ at 293 K. In each image, the domains that form are darker than the background.

of fluence results in permanent changes in the magnetic response.

Figure 6 shows the effect of laser excitation at 330 K for sample B at remanence after the magnetic state was first prepared by application and removal of a saturating field. The laser beam was swept across the sample surface by rotating a mirror before the induced change in magnetic contrast was imaged by WFKM. Due to a small but nonvanishing difference in remanent Kerr signal between the ferromagnetic layers in proximity to the compensation temperature T_M, the Kerr contrast between the two types of AP domain is relatively small. Improved contrast was obtained by subtracting an image of a monodomain AP state at remanence. The subtraction removes defects and other nonmagnetic features from the image.

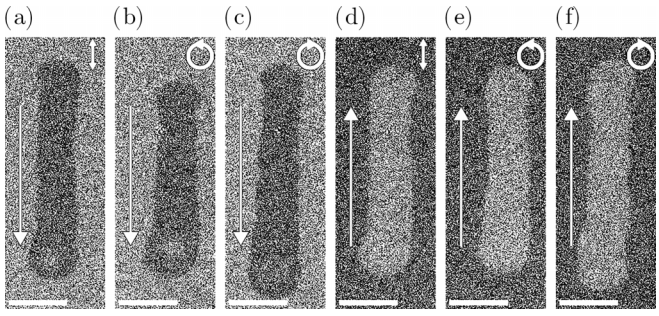

FIG. 6. WFKM images of HI-AOS from $\mathbf{AP}^+$ to $\mathbf{AP}^-$ in SFi sample B at 330 K using (a), (d) LP light of fluence 3.0 mJ/cm^2, (b), (e) LCP, and (c), (f) RCP light of fluence 4.1 mJ/cm^2, with 1035 nm wavelength, 10 ps pulse width and 1 MHz pulse repetition rate. (a)–(c) show switching when the remanent state is prepared using a saturating field of +104 mT, whereas (d)–(f) show switching when a saturating field of −104 mT is used. The beam was swept at a rate of approximately 150 μm/s, in the direction indicated by the arrow. Scale bars in the bottom left show a 50 μm length.

HI-AOS is shown for excitation by right and left circularly polarized (RCP, LCP) light [Figs. 6(b), 6(c) 6(e), and 6(f)] above the fluence threshold, and for linearly polarized (LP) light [Figs. 6(a), 6(d)] at a somewhat reduced fluence that accounts for the increased reflection coefficient relative to CP light when the pump beam has 45° angle of incidence. Above T^B_{-R} HI-AOS does not occur, and changes to the magnetic contrast are consistent with thermal demagnetization. HI-AOS is also found for sample A up to 289 K (see Fig. S8 [32]). Unlike in sample B however, above T^A_{-R}, changes to the magnetic contrast resulting from laser exposure become negligible, and neither HI-AOS nor thermal demagnetization occur. In general, full AOS is most likely to be observed as the temperature is increased to just below T_{-R}. However, the contrast between AP states declines rapidly, making it increasingly difficult to determine the magnetic state after laser exposure. The reduction in contrast comes about due to the temperature dependence of Kerr signal in the FM layers, resulting in a compensation temperature for the Kerr signal (where contrast is minimized) that often appears in the vicinity of T_M.

The value of T_{-R} determined by WFKM was found to depend on the speed at which the applied field was swept. The temperature at which positive remanence behavior is seen can be increased by slowing the field sweep rate in hysteresis measurements (see Figs. S1–S3 [32]). Minor differences in T_{-R} values determined by SQUID and WFKM measurements are likely to arise for this reason, with additional uncertainty arising from the calibration of the temperature sensors in the two systems. The global nature of SQUID measurements is also in contrast to the local nature of WFKM measurements,

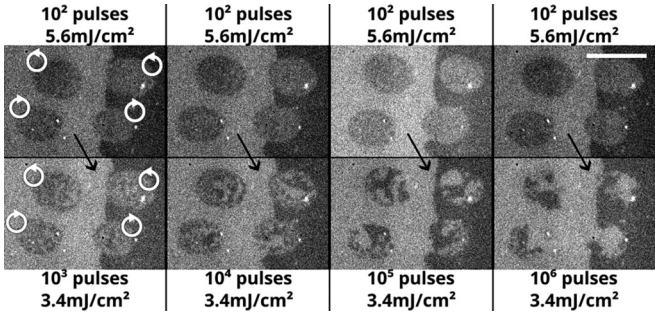

FIG. 7. WFKM images of two step excitation of sample A at 250 K. The result of initial exposure to a beam with high fluence (5.6 mJ/cm^2) is shown in the top row. Further changes induced by a beam of lower fluence (3.4 mJ/cm^2) are shown in the bottom row. Successive images in the bottom row show the effect of increasing the number of pulses in the second step by a factor of 10 from 10^3 (left) to 10^6 (right). In each image, a domain wall from top to bottom separates $\mathbf{AP^+}$ on the left from $\mathbf{AP^-}$ on the right. The elliptical circular regions at the top of each image were exposed to LCP light, while the bottom two were exposed to RCP light. The repetition rate and pulse width were 1 MHz and 280 fs, respectively. The scale bar at the top right has 50 μm length.

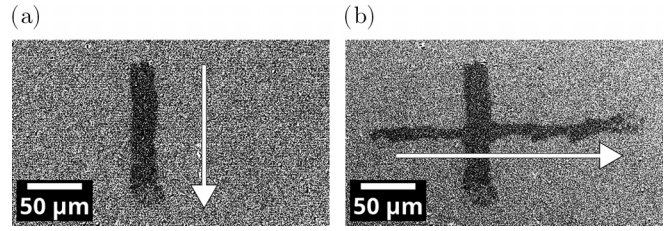

FIG. 8. WFKM images of sample B at 325 K, (a) following an initial vertical scan of a 1035 nm wavelength, 10 ps pulse duration, 1 MHz repetition rate linearly polarized beam with fluence of 1.9 mJ/cm^2, and (b) after an additional horizontal scan of a beam with the same parameters across the vertically swept region. The swept regions show AOS from $\mathbf{AP^+}$ to $\mathbf{AP^-}$, but the reverse switching is not found at the intersection of the two scans.

for which sample properties can be expected to vary slightly between different areas of the sample due to nonuniformity or the presence of defects.

Figure 7 shows the effect of a two-step excitation process with a stationary laser beam, where exposure to 10^2 high fluence pulses was followed by exposure to a variable number of lower fluence pulses. AOS is not achieved here but the results illustrate the evolution of the magnetic state during the pulsing process. Any domains present after the first step are too small to be resolved and a grayscale value halfway between that of the $\mathbf{AP^+}$ and $\mathbf{AP^-}$ states is observed. After the second step, domains are seen within the demagnetized regions that increase in size as more low fluence pulses are applied. This suggests that HI-AOS takes place in two stages. First, a thermally demagnetized region is formed, while second, domains grow due to a more moderate transient increase in temperature, with domains with switched magnetization finally dominating.

The AOS seen in the present SFi samples differs from that seen in other systems. Figure 8(a) shows AOS in sample B induced by a 1.9 mJ/cm^2 linearly polarized beam swept from top to bottom at a rate of approximately 150 μm/s. This is followed in Fig. 8(b) by a similar beam being swept from left to right, across the initially switched region, and shows that at the intersection of the swept regions, there is no toggle switching back to the initial AP state. Instead, the switching is unidirectional and to reinitialize the state for AOS in either direction requires the application and removal of a saturating field between measurements.

Further investigation showed that the capacity for AOS is significantly affected by the field history. A saturating field was applied in one direction and removed, before a much smaller field was applied in the opposite direction and removed. Even though the same initial AP state was obtained, this latter small field was found to hinder AOS and instead promote formation of a demagnetized state in swept beam experiments (see Figs. S9 and S10 [32]).

VII. DISCUSSION

The range of temperatures for which negative remanence is observed is significantly reduced from approximately $\Delta T_{-R}^{\mathrm{Ni_3Pt}} \approx 50$ K for SFi's with an alloy layer to $\Delta T_{-R}^{\mathrm{[Ni/Pt]}} \approx 20$ K for [Ni/Pt]-based SFi's. The transition between positive and negative remanence at the negative remanence temperature is also more sudden. Both these observations suggest that the [Ni/Pt] samples are more spatially homogeneous and have better structural quality as a result of the modified growth procedure. In both systems, temperature plays a large role in AOS, which is only observed below the negative remanence temperature. The negative remanence behavior arises due to the relative size of the magnetic anisotropy of the ferromagnetic layers, which is inferred to be temperature dependent due to the occurrence of the phenomenon over a finite range of temperatures. Presumably the optically induced modification of magnetic anisotropy in the two ferromagnetic layers is also important in the processes that result in AOS. It is also possible that stray field from surrounding film has some influence on the remagnetization process.

Switching of the SFi's is thought to be mediated by the flow of spin current through the Ir spacer layer, resulting in part from the different rates of ultrafast demagnetization in the FM layers [31]. Additionally, the importance of domain growth is underlined by the dependence of domain size upon the number of optical pulses seen in Fig. 7. Sweeping the beam across the sample is found to be the most robust means of inducing AOS. The two-step switching observed in Fig. 7 may be one of the reasons the swept beam is effective as first the higher fluence inner region of a Gaussian beam causes thermal demagnetization, followed by stimulation by the lower fluence outer region to promote domain growth. We observe the remagnetization of thermally demagnetized areas shown in the second step. The mechanism behind this process of domain growth is not yet fully understood and requires further study, but could involve the generation of hot nonthermal electrons throughout the duration of a laser pulse, of either fs or ps duration, which can give rise to superdiffusive

spin currents that induce magnetization dynamics as in Ref. [41].

The unidirectional nature of the HI-AOS suggests the possible presence of nanoscale magnetic texture that is related to the magnetic field history, but is not resolved due to the finite spatial resolution of the WFKM. This texture may promote the growth of domains in which the magnetization is switched relative to the direction of the original saturating magnetic field, and then pin the switched magnetization so as to prevent optically induced switching back to the initial state. The magnetic pinning and corresponding ability to switch are strongly influenced by even small fields applied prior to optical exposure, and in fact subtle changes in the magnetic state can be observed within quasistatic hysteresis loops as a small inflection in the signal when passing through the remanent state at temperatures below T_{-R} (see Fig. S11 [32]). The ability of the magnetic field to induce and remove the putative underlying magnetic texture contrasts with the inability to erase it optically, establishing a fundamental difference between switching induced by a magnetic field on one hand and optical excitation on the other. Nevertheless, the ability to reset the magnetic state through application of a magnetic field shows that optical excitation does not lead to irreversible structural changes within the sample.

VIII. CONCLUSIONS

In summary, unidirectional multipulse HI-AOS between AP states has been observed in [Ni/Pt]-based SFi's for temperatures up to 330 K. This is a significant increase in the temperature at which AOS can be realized when compared to the SFi's containing Ni_3Pt alloy layers in Ref. [31] and is approaching the operating temperature within conventional magnetic hard disk technology. SFi's based on [Ni/Pt] exhibit increased interlayer exchange coupling and both the negative remanence and compensation temperatures may be increased by reducing the Pt layer thickness. On the other hand, the AOS was found to be unidirectional and sensitive to the detailed magnetic field history. AOS was most easily achieved by sweeping the laser beam across the sample, which is consistent with two-step fixed-beam measurements where a high fluence followed by a low fluence was found to promote growth of domains. Preference for the switched state, and resistance to optically induced switching back to the original state, suggest the presence of nanoscale magnetic texture that cannot be resolved with an optical microscope. Further work is now needed to image the optically induced state with higher spatial resolution using techniques such as x-ray photoemission electron microscopy (XPEEM), so that nanoscale magnetic texture can be observed, understood, and then controlled to yield more robust HI-AOS.

All the data supporting the findings of this study are available within the paper and the Supplemental Material and have been deposited in Open Research Exeter (ORE) repository [42].

ACKNOWLEDGMENTS

This work was supported by the Engineering and Physical Sciences Research Council (EPSRC) under Grants No. EP/W006049/1, No. EP/P021190/1, No. EP/P020151/1, No. EP/P02047X/1, and No. EP/W006006/1. C.R.J.S. and D.G.N. acknowledge support via the EPSRC Centre for Doctoral Training in Metamaterials under Grant No. EP/L015331/1. R.M.B. and W.R.H. acknowledge the support of Seagate Technology (Ireland) under SOW #00077300.0. R.M.B. and J.N.S. acknowledge the support of the Royal Academy of Engineering under the Research Chairs and Senior Research Fellowships Scheme. This research used the resources of the Exeter Time-Resolved Magnetism Facility (EXTREMAG - EPSRC Grant Reference No. EP/R008809/1 and No. EP/V054112/1), and of the Advanced Light Source, which is a DOE Office of Science User Facility under Contract No. DEAC02-05CH11231. Diamond Light Source is acknowledged for beamtime on I10 under Project No. MM30343. For the purpose of open access, the authors have applied a Creative Commons Attribution (CC BY) license to any Author Accepted Manuscript version arising.

[1] R. F. L. Evans, R. W. Chantrell, U. Nowak, A. Lyberatos, and H.-J. Richter, Appl. Phys. Lett. **100**, 102402 (2012).

[2] C. S. Davies, J. H. Mentink, A. V. Kimel, T. Rasing, and A. Kirilyuk, J. Magn. Magn. Mater. **563**, 169851 (2022).

[3] E. Beaurepaire, J. C. Merle, A. Daunois, and J. Y. Bigot, Phys. Rev. Lett. **76**, 4250 (1996).

[4] A. R. Khorsand, M. Savoini, A. Kirilyuk, A. V. Kimel, A. Tsukamoto, A. Itoh, and Th. Rasing, Phys. Rev. Lett. **108**, 127205 (2012).

[5] Y. Quessab, M. Deb, J. Gorchon, M. Hehn, G. Malinowski, and S. Mangin, Phys. Rev. B **100**, 024425 (2019).

[6] C.-H. Lambert, S. Mangin, B. S. S. Varaprasad, Y. K. Takahashi, M. Hehn, M. Cinchetti, G. Malinowski, K. Hono, Y. Fainman, M. Aeschlimann, and E. E. Fullerton, Science **345**, 1337 (2014).

[7] M. S. El Hadri, M. Hehn, P. Pirro, C.-H. Lambert, G. Malinowski, E. E. Fullerton, and S. Mangin, Phys. Rev. B **94**, 064419 (2016).

[8] R. John, M. Berritta, D. Hinzke, C. Müller, T. Santos, H. Ulrichs, P. Nieves, J. Walowski, R. Mondal, O. Chubykalo-Fesenko, J. McCord, P. M. Oppeneer, U. Nowak, and M. Münzenberg, Sci. Rep. **7**, 4114 (2017).

[9] U. Parlak, R. Adam, D. E. Bürgler, S. Gang, and C. M. Schneider, Phys. Rev. B **98**, 214443 (2018).

[10] G. Kichin, M. Hehn, J. Gorchon, G. Malinowski, J. Hohlfeld, and S. Mangin, Phys. Rev. Appl. **12**, 024019 (2019).

[11] K. T. Yamada, A. V. Kimel, K. H. Prabhakara, S. Ruta, T. Li, F. Ando, S. Semin, T. Ono, A. Kirilyuk, and T. Rasing, Front. Nanotechnol. **4**, 765848 (2022).

[12] S. Mangin, M. Gottwald, C.-H. Lambert, D. Steil, V. Uhlíř, L. Pang, M. Hehn, S. Alebrand, M. Cinchetti, G. Malinowski, Y. Fainman, M. Aeschlimann, and E. E. Fullerton, Nature Mater. **13**, 286 (2014).

[13] J.-W. Liao, P. Vallobra, L. O'Brien, U. Atxitia, V. Raposo, D. Petit, T. Vemulkar, G. Malinowski, M. Hehn, E. Martínez,

S. Mangin, and R. P. Cowburn, Adv. Sci. **6**, 1901876 (2019).
[14] I. Radu, K. Vahaplar, C. Stamm, T. Kachel, N. Pontius, H. A. Dürr, T. A. Ostler, J. Barker, R. F. L. Evans, R. W. Chantrell, A. Tsukamoto, A. Itoh, A. Kirilyuk, T. Rasing, and A. V. Kimel, Nature (London) **472**, 205 (2011).
[15] C. E. Graves, A. H. Reid, T. Wang, B. Wu, S. de Jong, K. Vahaplar, I. Radu, D. P. Bernstein, M. Messerschmidt, L. Müller, R. Coffee, M. Bionta, S. W. Epp, R. Hartmann, N. Kimmel, G. Hauser, A. Hartmann, P. Holl, H. Gorke, J. H. Mentink *et al.*, Nature Mater. **12**, 293 (2013).
[16] J. Barker, U. Atxitia, T. A. Ostler, O. Hovorka, O. Chubykalo-Fesenko, and R. W. Chantrell, Sci. Rep. **3**, 3262 (2013).
[17] C. D. Stanciu, F. Hansteen, A. V. Kimel, A. Kirilyuk, A. Tsukamoto, A. Itoh, and Th. Rasing, Phys. Rev. Lett. **99**, 047601 (2007).
[18] K. Vahaplar, A. M. Kalashnikova, A. V. Kimel, D. Hinzke, U. Nowak, R. Chantrell, A. Tsukamoto, A. Itoh, A. Kirilyuk, and Th. Rasing, Phys. Rev. Lett. **103**, 117201 (2009).
[19] T. A. Ostler, J. Barker, R. F. L. Evans, R. W. Chantrell, U. Atxitia, O. Chubykalo-Fesenko, S. El Moussaoui, L. Le Guyader, E. Mengotti, L. J. Heyderman, F. Nolting, A. Tsukamoto, A. Itoh, D. Afanasiev, B. A. Ivanov, A. M. Kalashnikova, K. Vahaplar, J. Mentink, A. Kirilyuk, T. Rasing *et al.*, Nat. Commun. **3**, 666 (2012).
[20] A. Hassdenteufel, B. Hebler, C. Schubert, A. Liebig, M. Teich, M. Helm, M. Aeschlimann, M. Albrecht, and R. Bratschitsch, Adv. Mater. **25**, 3122 (2013).
[21] A. Kirilyuk, A. V. Kimel, and T. Rasing, Rep. Prog. Phys. **76**, 026501 (2013).
[22] M. L. M. Lalieu, M. J. G. Peeters, S. R. R. Haenen, R. Lavrijsen, and B. Koopmans, Phys. Rev. B **96**, 220411(R) (2017).
[23] J. Gorchon, C.-H. Lambert, Y. Yang, A. Pattabi, R. B. Wilson, S. Salahuddin, and J. Bokor, Appl. Phys. Lett. **111**, 042401 (2017).
[24] Y. L. W. van Hees, P. van de Meugheuvel, B. Koopmans, and R. Lavrijsen, Nat. Commun. **11**, 3835 (2020).
[25] S. Iihama, Y. Xu, M. Deb, G. Malinowski, M. Hehn, J. Gorchon, E. E. Fullerton, and S. Mangin, Adv. Mater. **30**, 1804004 (2018).
[26] C. Banerjee, N. Teichert, K. E. Siewierska, Z. Gercsi, G. Y. P. Atcheson, P. Stamenov, K. Rode, J. M. D. Coey, and J. Besbas, Nat. Commun. **11**, 4444 (2020).
[27] A. Stupakiewicz, K. Szerenos, D. Afanasiev, A. Kirilyuk, and A. V. Kimel, Nature (London) **542**, 71 (2017).
[28] J. Igarashi, W. Zhang, Q. Remy, E. Díaz, J.-X. Lin, J. Hohlfeld, M. Hehn, S. Mangin, J. Gorchon, and G. Malinowski, Nature Mater. **22**, 725 (2023).
[29] M. Dąbrowski, S. Guo, M. Strungaru, P. S. Keatley, F. Withers, E. J. G. Santos, and R. J. Hicken, Nat. Commun. **13**, 5976 (2022).
[30] R. F. L. Evans, T. A. Ostler, R. W. Chantrell, I. Radu, and T. Rasing, Appl. Phys. Lett. **104**, 082410 (2014).
[31] M. Dąbrowski, J. N. Scott, W. R. Hendren, C. M. Forbes, A. Frisk, D. M. Burn, D. G. Newman, C. R. J. Sait, P. S. Keatley, A. T. N'Diaye, T. Hesjedal, G. van der Laan, R. M. Bowman, and R. J. Hicken, Nano Lett. **21**, 9210 (2021).
[32] See Supplemental Material at http://link.aps.org/supplemental/10.1103/PhysRevB.109.134417 for details on the temperature-dependent behavior of [Ni/Pt] reference layers, WFKM loops, and domain images of Co reference layers, SQUID, XMCD, and WFKM measurements to show the remanence, element specific, and AOS properties, respectively, of SFi sample A, the formation of AP domains in [Ni/Pt]-based SFi's at temperatures close to T_{-R}, and the effect of a historical bias field on the capacity for AOS.
[33] R. B. Morgunov, E. I. Kunitsyna, A. D. Talantsev, O. V. Koplak, T. Fache, Y. Lu, and S. Mangin, Appl. Phys. Lett. **114**, 222402 (2019).
[34] S. S. P. Parkin, Phys. Rev. Lett. **67**, 3598 (1991).
[35] A. Dinia, M. Stoeffel, K. Rahmouni, D. Stoeffler, and H. A. M. van den Berg, Europhys. Lett. **42**, 331 (1998).
[36] M. S. Gabor, T. Petrisor, R. B. Mos, M. Nasui, C. Tiusan, and T. Petrisor, J. Phys. D **50**, 465004 (2017).
[37] Q. Ma, Y. Li, Y.-s. Choi, W.-C. Chen, S. J. Han, and C. L. Chien, Appl. Phys. Lett. **117**, 172403 (2020).
[38] K. Takanashi, H. Kurokawa, and H. Fujimori, Appl. Phys. Lett. **63**, 1585 (1993).
[39] C. R. J. Sait, Ph.D. thesis, University of Exeter, 2023, https://ore.exeter.ac.uk/repository/handle/10871/133977.
[40] P. J. H. Bloemen, H. W. Van Kesteren, H. J. Swagten, and W. J. M. de Jonge, Phys. Rev. B **50**, 13505 (1994).
[41] D. Rudolf, C. La-O-Vorakiat, M. Battiato, R. Adam, J. M. Shaw, E. Turgut, P. Maldonado, S. Mathias, P. Grychtol, H. T. Nembach, T. J. Silva, M. Aeschlimann, H. C. Kapteyn, M. M. Murnane, C. M. Schneider, and P. M. Oppeneer, Nat. Commun. **3**, 1037 (2012).
[42] https://ore.exeter.ac.uk/repository/handle/10871/135632.